Vascular design for thermal management of heated structures

J. Lee
Duke University
Department of Mechanical Engineering and Materials Science
Durham, North Carolina
USA

S. Lorente
University of Toulouse, INSA, Laboratory of Materials and Durability of Constructions
Toulouse
France

A. Bejan
abejan@duke.edu
Duke University
Department of Mechanical Engineering and Materials Science
Durham, North Carolina
USA

ABSTRACT

Vascular structures are contemplated for cooling the skins and leading surfaces of future high speed aircraft. This paper evaluates the proposal to cool with a flow architecture shaped as trees (dendritic) a parallelepipedic body that is heated uniformly. The coolant enters the body through one face and exits through the opposite face. The vasculature connects the two faces, and consists of trees that alternate with upside down trees. The fields for fluid flow and heat transfer are determined numerically in three dimensions. The effect of local pressure losses at bends, junctions and entrances is documented. Designs with tree-shaped architectures having up to four levels of bifurcation are evaluated for fluid flow and heat transfer performance, and are compared with the performance of a design with a single sheet of fluid sweeping the upper surface of the body. The fluid flow conductance of the tree designs increases when the number of bifurcation levels increases. The thermal performance of tree designs can be improved by endowing the tree design with more freedom such that the bifurcations generate asymmetric daughter channels. The tree designs outperform the fluid sheet design dramatically: the global thermal resistance of the tree designs is roughly one tenth of the global thermal resistance of the fluid sheet design.

NOMENCLATURE

A	area, m^2
Be	Bejan number, Equation (22)
C	criterion length for avoiding interference between adjacent trees, m
c_p	specific heat capacity, J kg^{-1} K^{-1}
d	elemental length, m, Fig. 2
D	channel diameter, m
h	depth of channels, m, Fig. 2
i	order of bifurcating levels
k	thermal conductivity, W kg^{-1} K^{-1}
$\tilde{k}$	ratio of conductivities, k_s/k_f
L_i	channel length, m
$\dot{m}$	mass flow rate, Kg s^{-1}
$\dot{m}'$	mass flow rate per unit length, kg s^{-1} m^{-1}
M	dimensionless mass flow rate, Equation (28)
n	number of channels of the same size per bifurcating level, or unit outward normal vector at surface
p	number of bifurcating levels
p	pressure, Pa
P	pumping power, W, Equation (25)
Pr	Prandtl number, Pr = ν/α
q	total heat current, W
q''	heat flux,
$\tilde{R}$	dimensionless thermal resistance, Equations (23) and (24)

Paper No. 3322. Manuscript received 28 July 2008, accepted 13 January 2009.

https://doi.org/10.1017/S0001924000003067 Published online by Cambridge University Press

S	width of rectangular cross section of channels, m
Sv	svelteness number, Equation (1)
t	wall thickness between channels and wall, m, Fig. 2
T	temperature, K
v	velocity, m s^{-1}
V	total volume, m^3
V_c	total flow volume, m^3
X, Y, W	dimensions of tree-shaped structure, m, Fig. 2
x	co-ordinate, m
$\tilde{W}$	dimensionless pumping power requirement, Equation (29)

Greek symbols

α	thermal diffusivity of fluid, $m^2 s^{-1}$
ΔP	pressure difference, *Pa*
δ	thickness of parallel-plate sheet
μ	dynamic viscosity,
ρ	density,
ν	kinematic viscosity,
ϕ	porosity, Equation (9)

Subscripts

f	fluid
i	channel rank
in	inlet
j, k	indices, Einstein summation convention
max	maximum
min	minimum
0	reference
out	outlet
s	solid
u	upper surface on plane in Fig. 2

Superscripts

$\tilde{(\ )}$	dimensionless

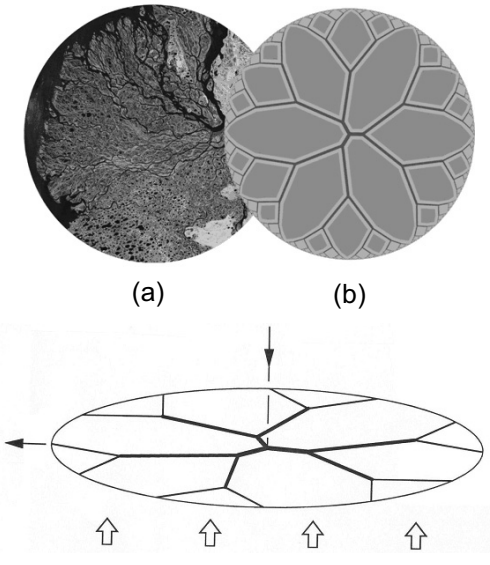


Figure 1. The two sides of the constructal theory coin: with constructal theory we predict the occurrence of design in nature, and we design with strategy (faster, for greater flow performance) devices for human use. Figure (a) shows an example of tree-shaped design in nature: the delta of the river Lena in northern Siberia. Figure (b) shows the constructal delta-like architecture that connects the center with ports on the disc perimeter. The lower sketch shows how a point-circle vascular body can fight the intense heating that impinges on its flat side.

1.0 THERMAL MANAGEMENT WITH VASCULAR MATERIALS

New research spanning the entire spectrum from biology to geophysics is showing a renewed interest in the principles that guide the design of tree-shaped flow architectures. The reason is the emergence of tree architectures as the most effective (most direct, efficient, with less resistance) flow connections between discrete points and continua (curves, areas, volumes): the fluid-flow performance of complex trees is superior to that of parallel channels. This body of work is coming together as constructal theory[1-5], which is the view that the occurrence and evolution of design in nature is a physics phenomenon that should proceed in accordance with the constructal law[2]: 'For a finite-size flow system to persist in time (to live) it must evolve such that it provides easier and easier access to its currents'. According to the constructal law, freely morphing flow systems have a universal tendency to evolve in time as a sequence of easier flowing configurations. The constructal law is the principle of life and evolution in physics[6]. As an example, tree-shaped flows are discovered (deduced)[2,3,7] from the constructal law, not by observing and copying nature. This work was reviewed most recently in Refs.[1,4-6].

The principle of how flow configurations are generated is useful in two domains. First, the principle allows us to explain and predict the occurrence of flow design in nature (for example, a river delta, Fig. 1(a). This theoretical view offers a physics basis for the phenomenon of evolution that dominates not only biological design[2,3] but also geophysical design (e.g. river basin evolution[5, 6]) and societal design (e.g. urban traffic, air transportation, internet). Second, principles allow us to engineer novel flow architectures that are better than the designs tried until now (for example, delta-like vasculatures for cooling discs that generate heat, Fig. 1(b)). They guide us to design more directly, faster, and with strategy. The engineering side of constructal theory is developing in several directions in which dendritic flow designs are the new configurations. Examples are the cooling of electronics[8-11], the configuring of fuel cells[12,13], and the vascularisation of materials with self-healing functionality[14, 15].

In this paper we explore another important volumetric functionality that can be implemented by using tree vascularisation: volumetric cooling and surface cooling. This is a fundamental process for the design of thermal management of the skins and leading surfaces of future aircraft. The most fundamental question is whether tree-shaped vasculatures are more effective for cooling than parallel channels.

We consider this fundamental problem in the three-dimensional slab configuration shown in Fig. 2. Heat is generated uniformly over the area at the rate q'' The coolant sweeps the area from side to side. The vasculature for this sweep consists of trees that alternate with upside down trees, in accordance with the line-to-line trees proposed in Ref. 16. Trees that alternate with 'upside down trees' is an expression made with reference to botanical trees, which are all upright, with water flow upward, from trunk to canopy. When some of the trees are upside down, and the flow is from canopy to trunk, the flow is still upward, as in the upright trees: Put together, the naturally oriented trees and the upside down trees form an architecture that flows upward, from a bottom line (plane) to an upper line (plane). See Fig. 2.

In Ref. 16 it was shown that the advantage of line-to-line trees in comparison with transversal parallel channels is that they offer a smaller global flow resistance when the smallest length scales are small enough so that the number of pairing levels in the tree structure is greater than four. Here we investigate the convective cooling performance of the line-to-line tree structure.

2.0 GEOMETRY

The geometrical features of the flow architecture are defined in Fig. 2. Each tree is designed in accordance with the minimal-lengths tree design proposed in Ref. 17, which yielded 90° angles at every bifurcation level. Although the minimal-lengths trees are approximate (near optimal), their fluid flow performance comes surprisingly close to that of the fully

https://doi.org/10.1017/S0001924000003067 Published online by Cambridge University Press

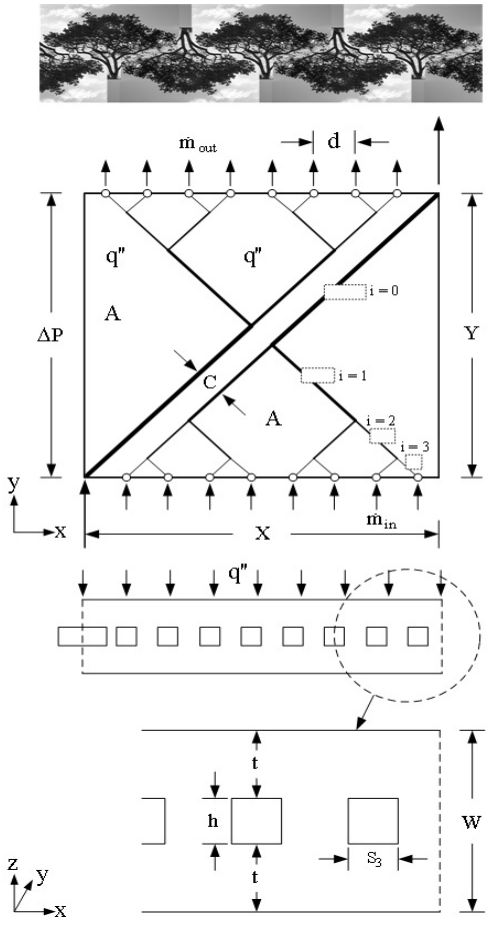


Figure 2. Line-to-line tree architecture, as a sequence of point-to-line trees alternating with upside down point-to-line trees.

optimised tree architectures. For example, the global flow resistance of a minimal-lengths tree with fully developed laminar flow and one level of pairing (a Y-shaped construct) exceeds by only 0·5 percent the global flow resistance of the fully optimised Y construct[16].

Because of the 90° angles, the outer branch of every bifurcation is collinear with the stem. The asymmetry of the Y makes the splitting of the stream unequal, with more fluid flowing along the collinear paths. This flow imbalance becomes more accentuated when the svelteness of the architecture Sv is less than 10, because in this domain the local pressure losses (junctions, bends, entrances) are not negligible. The svelteness is a global geometric property of the architecture[18],

$$Sv = \frac{\textit{external flow length scale}}{\textit{internal flow length scale}} = \frac{Y}{V_c^{1/3}} \qquad \ldots (1)$$

where V_C is the total volume of the flow channels. We will show that the flow imbalance downstream from a bifurcation is beneficial for convective cooling, because with larger flow rates through the outer channels of each bifurcation the tree is more effective in convecting away the heat generated by the larger subvolumes residing on the outer sides of the outer channels (e.g., areas '*A*' in Fig. 2).

The lengths of all the channels in a line-to-line tree with p pairing levels are;

$$L_i = 2^{p-i-1/2} d, \quad (i = 0, 1, ..., p) \qquad \ldots (2)$$

where d is the spacing between two adjacent ports of the tree canopy. Here d is the smallest detail that is visible from the outside of the vascularised slab. The smallest length scale is specified. The length of the tree in the flow direction is Y. The thickness of the vascularised conducting body (W) is equal to $d/4 = 1{\cdot}25$mm in Table 1. The distance between two adjacent trees (C) is also comparable with d. The design of the layout must be executed with care so that tree-tree interference ($C < 0$) is avoided.

The number of channels of the same size in a single tree is $n_i = 2^i$, ($i = 0, 1, ..., p$). The channel cross-sections are rectangular, $h \times S_i$ The manufacturing of such channels is easier when all the channels have the same depth (h). The channel widths (S_i) are selected based on a very effective rule derived from the classical Hess-Murray rule for bifurcation round tubes of diameters $D_i > D_{i+1}$[1,19,20]:

$$\frac{D_i}{D_{i+1}} = 2^{1/3} \qquad \ldots (3)$$

Written in terms of tube cross-sectional areas $A_i = \pi D_i^2/4$ the Hess-Murray rule is;

$$\frac{A_i}{A_{i+1}} = 2^{2/3} \qquad \ldots (4)$$

Rule (4) is adopted in the present design, and, because $A_i = hS_i$, this rule yields the sequence of rectangular channels widths

$$\frac{S_{i+1}}{S_i} = 2^{-2/3} = 0{\cdot}63 \qquad \ldots (5)$$

This rule is approximate. One can optimise numerically every S_{i+1}/S_i ratio so that the global flow resistance of the tree is minimal. We performed this numerical optimisation in Ref. 21, where we showed that the approximate rule[5] yields flow resistances that approach within 5·5 percent the fully minimised flow resistances. Because the best of all rectangular cross-sections is the square, the shape chosen for the smallest cross-sections ($i = p$) is square. This is the shape of the small ports through which the tree canopy communicates with the outside (Fig. 2, bottom).

The streamwise and transversal length scales of one tree are;

$$X = \left(2^p + \frac{1}{2}\right)d, \quad Y = \left(2^p - \frac{1}{2}\right)d \qquad \ldots (6)$$

which means that when p is large the $X \times Y$ element is almost square. The thickness of the thinnest wall of solid material is t, which means that the third dimension of the slab is;

$$W = h + 2t \qquad \ldots (7)$$

The total flow volume

$$V_c = 2\sum_{i=0}^{p} 2^i S_i h L_i \qquad \ldots (8)$$

is used for calculating the svelteness Sv Equation (1), and the void fraction, or porosity of the vascularised body

$$\phi = \frac{V_c}{V} \qquad \ldots (9)$$

where the element volume is $V = XYW$. Porosity is a misnomer, because this vascular structure is not a porous medium in the classical sense. The volume fraction ϕ is a constraint for two reasons, both having to do with the fact that the vascular flow structure must perform on an aircraft. The total weight of the structure (mostly solid) must be constrained, and so must be the total volume (solid and fluid). These two constraints translate into having to fix ϕ. In the work reported here we used $\phi = 0{\cdot}02$. Vasculatures with larger ϕ values can be analysed in the same fashion: they would be easier to manufacture, but their mechanical strength would suffer.

https://doi.org/10.1017/S0001924000003067 Published online by Cambridge University Press

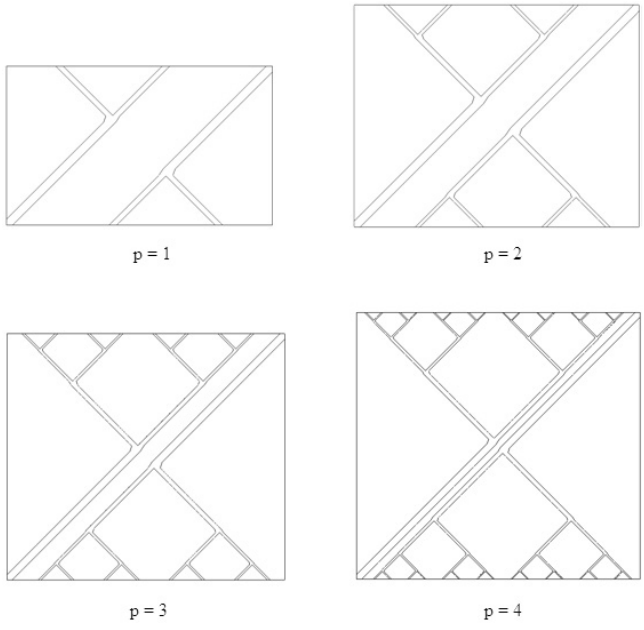


Figure 3. Line-to-line tree architectures with one, two, three and four levels of pairing.

In this work we studied many configurations, which can be thought of as configurations that populate a design space measured in terms of dimensionless parameters such as ϕ, p, Sv, etc. For illustration, the presentation is made in dimensional terms, with d = 0·5cm as the reference length scale, and $W = d/4$ = 0·125cm. The dimensions of the elemental tree (XY) increase as the number of pairing levels p increases. The dimensions of the resulting tree architectures are summarised in Table 1, where 'area' means channel cross-sectional area, and D_h is the hydraulic diameter of every channel.

Because the channels have finite widths (unlike in the upper drawing of Fig. 2), complex tree structures are possible only if ϕ is sufficiently small. The criterion for avoiding interference between adjacent trees is $(S_0/S_1)/2 < C$. Based on this criterion we constructed Table 2, which shows the design domain (p, ϕ, Sv) that we have explored, and the domain that is not accessible (indicated by ×). The table also shows the svelteness of each (p, ϕ) tree structure. The fact that is not much greater than 10 means that full numerical simulations of the flow were necessary in order to capture the details of the flow and pressure losses at all the junctions. The upper dashed line corresponds to Sv ~ 10 indicating that the cases shown in the upper-right of the table (small p large ϕ) have significant local pressure losses.

3.0 NUMERICAL MODEL

The numerical model is based on assuming steady, incompressible and laminar flow in every channel, and constant properties for the solid and the fluid. By using the Einstein summation convention, the equations for continuity, momentum and energy for the fluid space are expressed as;

$$\frac{\partial v_j}{\partial x_j} = 0 \qquad \ldots (10)$$

$$\rho\left(v_j \frac{\partial v_k}{\partial x_j}\right) = -\frac{\partial P}{\partial x_k} + \mu\left(\frac{\partial^2 v_k}{\partial x_j^2}\right) \qquad \ldots (11)$$

$$\rho c_p\left(v_j \frac{\partial T_f}{\partial x_j}\right) = k_f \frac{\partial^2 T_f}{\partial x_j^2} \qquad \ldots (12)$$

The energy equation for the solid space is;

$$\frac{\partial^2 T_s}{\partial x_j^2} = 0 \qquad \ldots (13)$$

The constant heat flux imposed on the upper XY plane is;

$$q'' = -k_s \left.\frac{\partial T_s}{\partial x_k}\right|_u \qquad \ldots (14)$$

The continuity of heat flux through the solid-fluid interfaces requires;

$$k_s \frac{\partial T_s}{\partial n_k} = k_f \frac{\partial T_f}{\partial n_k} \qquad \ldots (15)$$

The conjugate conduction and convection problem was nondimensionlised by introducing the dimensionless variables

$$\tilde{x}_k = x_k / Y, \qquad \tilde{v}_k = v_k Y / \nu$$
$$\tilde{P} = (P - P_0)Y^2/(\mu\alpha), \qquad \tilde{T} = (T - T_0)k_f/(q''Y) \qquad \ldots (16)$$

where P_0 and T_0 are the reference pressure and temperature, respectively. The dimensionless conservation equations become;

$$\frac{\partial \tilde{v}_j}{\partial \tilde{x}_j} = 0 \qquad \ldots (17)$$

$$\tilde{v}_j \frac{\partial \tilde{v}_k}{\partial \tilde{x}_j} = -\frac{1}{\mathrm{Pr}} \frac{\partial \tilde{P}}{\partial \tilde{x}_k} + \frac{\partial^2 \tilde{v}_k}{\partial \tilde{x}_j^2} \qquad \ldots (18)$$

$$\tilde{v}_j \frac{\partial \tilde{T}_f}{\partial \tilde{x}_j} = \frac{1}{\mathrm{Pr}} \frac{\partial^2 \tilde{T}_f}{\partial \tilde{x}_j^2} \quad \text{(fluid)} \qquad \ldots (19)$$

$$\frac{\partial^2 \tilde{T}_s}{\partial \tilde{x}_j^2} = 0 \quad \text{(solid)} \qquad \ldots (20)$$

$$\frac{1}{\tilde{k}} = -\left.\frac{\partial \tilde{T}_s}{\partial \tilde{x}_k}\right|_u, \qquad \tilde{k}\left(\frac{\partial \tilde{T}}{\partial \tilde{n}_k}\right)_s = \left(\frac{\partial \tilde{T}}{\partial \tilde{n}_k}\right)_f \qquad \ldots (21)$$

where Pr and $\tilde{k}$ represent the Prandtl number and the ratio of thermal conductivities ($\tilde{k} = k_s / k_f$), respectively. It must be said that the constant properties model used here for the fluid and solid regions is a choice made for illustrating the method and the vasculatures. The results are valid in dimensional terms provided that the temperature variation through the flow volume is small. This variation depends on the value of the imposed heat flux q'' and this variation must be checked. If the q'' is high such that the calculated temperature variation is of order 10^3K then an entirely different model must be used, with temperature dependent properties and phase change.

4.0 PERFORMANCE OF LINE-TO-LINE TREES

The heat and fluid flow in the vascularised body was simulated as a conjugate conduction and convection phenomenon that covers continuously the entire three-dimensional vascularised volume. The simulations were performed for structures with p = 1, …, 4, as illustrated in Fig. 3. The porosity was ϕ = 0·02 in all cases. The ratio of thermal conductivities $\tilde{k}$ emerges as a dimensionless parameter in the dimensionless formulation of conjugate heat transfer because of the continuity of heat flux across solid-fluid interfaces. The value $\tilde{k}$ was chosen because it corresponds to the solid-fluid combination of stainless steel (AISI 304) and liquid water at ambient conditions.

https://doi.org/10.1017/S0001924000003067 Published online by Cambridge University Press

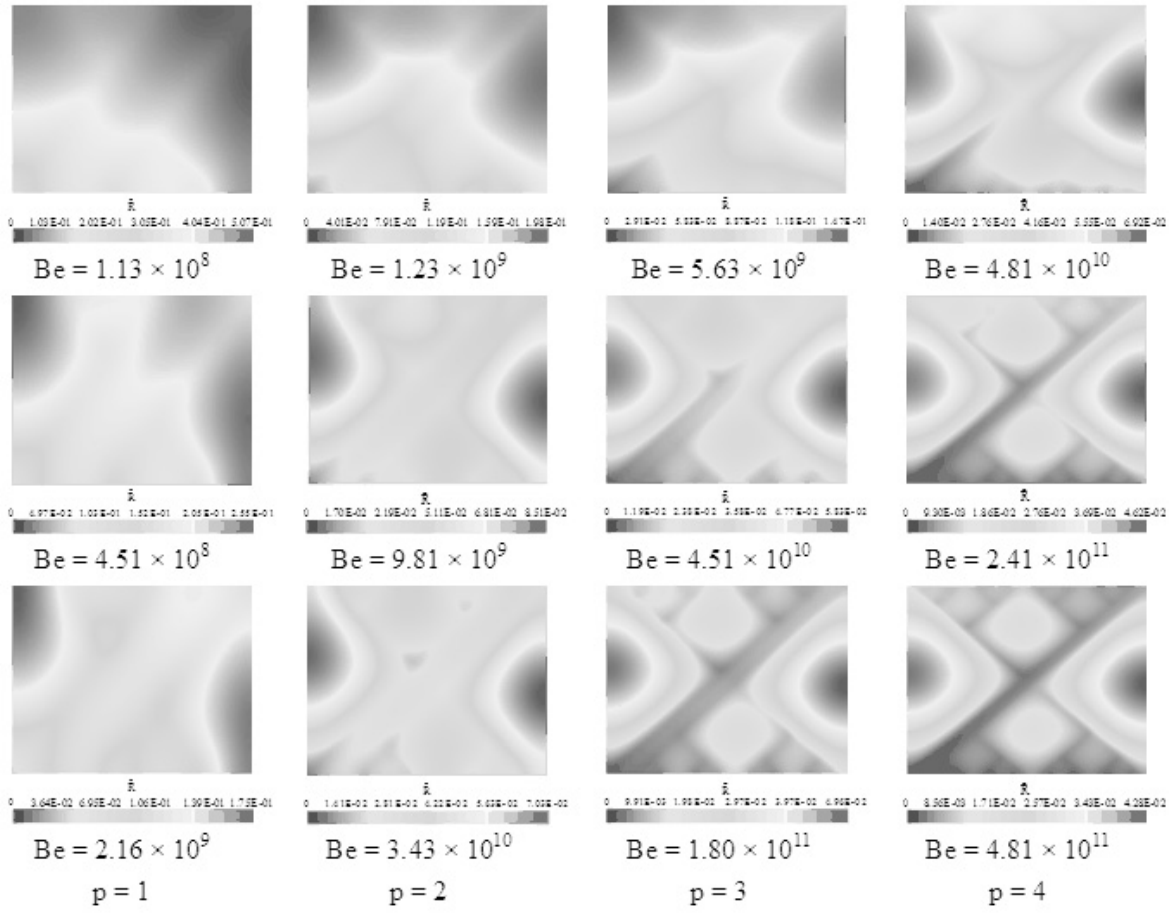


Figure 4. Dimensionless temperature distributions ($\tilde{R}$) in the structures of Fig. 3, showing the effect of pressure drop number (*Be*).

Table 1
Geometrical features of the tree-tree architecture of Fig. 2, with reference to *d* = 0·5cm (ϕ = 0·02)

p	*i*	*S* (mm)	L_i (mm)	*Area* (mm^2)	D_h (mm)	V_c (mm^3)	*V* (mm^3)	*Sv*	*X* (mm)	*Y* (mm)	*W* (mm)
1	1	0·25	3·5	0·064	0·25	2·3	117	5·6	12·5	7·5	1·25
	0	0·40	7·1	0·10	0·31						
2	2	0·26	3·5	0·068	0·26	9·8	492	8·2	22·5	17·5	1·25
	1	0·41	7·1	0·11	0·32						
	0	0·66	14·1	0·17	0·37						
3	3	0·29	3·5	0·077	0·28	39·8	1992	10·9	42·5	37·5	1·25
	2	0·44	7·1	0·12	0·34						
	1	0·70	14·1	0·19	0·40						
	0	1·10	28·3	0·31	0·45						
4	4	0·30	3·5	0·091	0·30	160	7992	14·3	82·5	77·5	1·25
	3	0·48	7·1	0·15	0·37						
	2	0·76	14·1	0·23	0·43						
	1	1·2	28·3	0·37	0·48						
	0	1·9	56·6	0·58	0·52						

https://doi.org/10.1017/S0001924000003067 Published online by Cambridge University Press

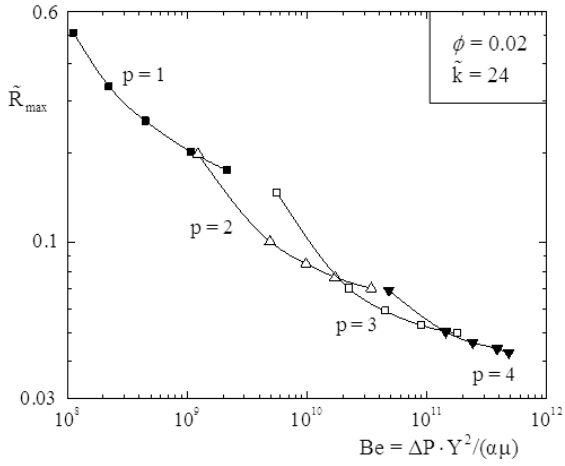


Figure 5. Numerical results for global thermal resistance *versus* pressure drop number (*Be*).

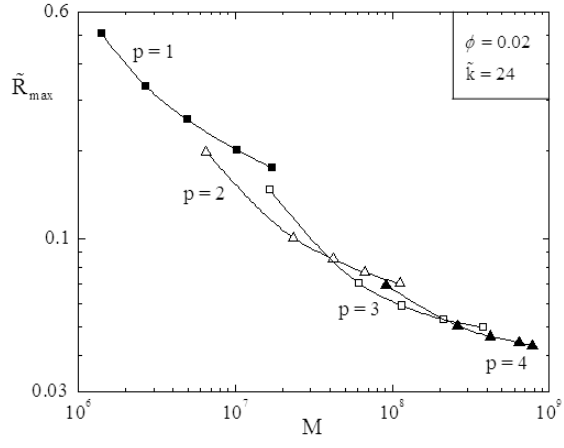


Figure 6. Numerical results for global thermal resistance *versus* dimensionless mass flow rate (*M*).

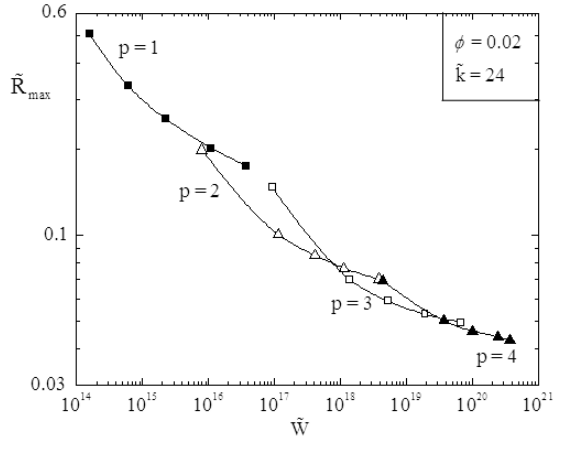


Figure 7. The competition between global thermal resistance ($\tilde{R}_{max}$) and dimensionless pumping power ($\tilde{W}$).

Table 2
The design domain *Sv*(*p*,ϕ) in which the channels of the two trees of Fig. 2 do not interfere. The numbers listed in the table indicate the value of *Sv*

p	ϕ					
	0·005	**0·01**	**0·02**	**0·03**	**0·04**	**0·05**
1	9·0	7·1	5·6	4·9	4·5	4·2
2	12·0	10·3	8·2	7·1	6·5	6·0
3	17·4	13·8	10·9	9·6	8·7	8·1
4	22·7	18·0	14·3	12·5	11·3	10·5
5	29·0	23·0	18·3	16·0	×	×
6	36·8	29·2	×	×	×	×
7	×	×	×	×	×	×

The pressure difference imposed from side to side was fixed by specifying the dimensionless pressure drop (called Bejan number by Bhattacharjee and Grosshandler[22] and Petrescu[23]),

$$Be = \frac{\Delta P \cdot Y^2}{\alpha\mu} \quad \ldots (22)$$

in the range 10^8-10^{12}, where α and μ are the thermal diffusivity and viscosity of water.

The numerical work was performed by using a finite-volume computational package[24]. The calculation of the temperature field was decoupled from the fluid flow field because the fluid is modeled as incompressible. The grid shape is triangular for both the fluid and solid domains. The first-order upwind discretisation scheme and simple-type algorithm were employed to calculate the fluid flow and temperature fields. Appropriate mesh sizes were selected in order to achieve accurate numerical results based on reasonable computational times. We used different mesh sizes for the fluid and solid domains. First, we selected the mesh size for the fluid flow field in order to satisfy the condition that the relative difference in the resulting overall mass flow rate (or global flow conductance) was less than one percent as the mesh size was decreased successively by 20 percent. Second, based on the mesh size for the fluid domain, the mesh size for the corresponding solid domain was determined from the criterion that the relative difference in the global maximum excess temperature (i.e., the hot spot temperature) was less than one percent as the mesh size was decreased successively by 20 percent. The fine mesh for the fluid domain and the coarse mesh for the solid domain were generated so that the overall mesh distributions of the tree-tree architectures in Fig. 3 were nonuniform. The reduction of grid size was applied to the control volumes until the relative difference in the mass flow rates was smaller than one percent as the successive grid sizes were refined by 20 percent. The meaning of 20 percent reduction of grid size is ambiguous without the general curve of the mass flow rates when the initially assumed grid number is given. For example, we used approximately 50,000 elements as the initial grid number for one tree with $p = 1$, and the trend of mass flow rates was made as a curve by decreasing the initial size in steps of 20 percent to determine a proper grid size. The grid size that satisfies the criterion depends on *Be* and pairing levels of bifurcation. The grid size was progressively finer as *Be* and the pairing levels increased.

During numerical simulations the pressure difference (*Be*) between fluid inlets and outlets was set so that the flow in all the channels was laminar (Re < 1,000) The uniform heat flux q'' lands perpendicularly on the upper *XY* plane, i.e., in the negative *z* direction in Fig. 2, perpendicular to the fluid flow. The vertical sides (*Y*) of the upper drawing of Fig. 2 are planes of symmetry. The other solid surfaces, the horizontal sides and the bottom plane, are adiabatic with respect to the exterior.

The effectiveness of tree-tree cooling is measured by how well the flow pattern depresses the peaks of highest temperature (the hot spots, T_{max}). The overall temperature difference across the *XYW* volume is

https://doi.org/10.1017/S0001924000003067 Published online by Cambridge University Press

($T_{max} - T_{min}$) where T_{min} is the inlet temperature of the coolant. The overall thermal resistance is $(T_{max} - T_{min})/q$, where q is the total heat current ($q''XY$). This global thermal resistance was nondimensionalised as;

$$\tilde{R}_{max} = \frac{T_{max} - T_{min}}{q'' Y^2 / (k_s W)} \quad \ldots (23)$$

The corresponding dimensionless temperature distribution is represented by

$$\tilde{R} = \frac{T - T_{min}}{q'' Y^2 / (k_s W)} \quad \ldots (24)$$

where $T(x,y,z)$ is the local temperature anywhere in the vascularised volume.

Figure 4 shows the dimensionless temperature distributions (Eqs (23, 24)) on the upper XY planes of the slab. Four designs are illustrated, $p = 1, \ldots, 4$. The hot spots tend to occur near the exit plane of the volume. They decrease in strength as the imposed pressure difference increases. When Be is sufficiently high, the hot spots move from the exit plane to the center of the largest interstices of the tree-tree network (e.g., areas 'A' in Fig. 2).

The effect of tree complexity or size (p or Y) and flow strength (Be) is summarised in Fig. 5. The hot spots diminish as the flow strength increases. The overall thermal resistance ($\tilde{R}_{max}$) for all the pairing levels decreases monotonically as Be increases. This trend is attractive, but it is accompanied by a negative effect: the pumping power required by the XYW element increases. The pumping power is;

$$\mathbf{P} = \dot{m} \Delta P / \rho \quad \ldots (25)$$

where $\dot{m}$ is the total flow rate through the X - wide side of the upper drawing in Fig. 2. The mass flow rate through one of the trees is closely approximated by $\dot{m}/2$. The reason why the two trees do not have exactly the same flow rates is the asymmetry of the flow through each bifurcation. The mass flow rate was nondimensionalised by writing in an order of magnitude sense that for Poiseuille flow in a duct of length Y and diameter D the pressure drop scales as

$$\Delta P \sim \frac{\dot{m} \nu Y}{D^4} \quad \ldots (26)$$

The channel diameter scale is related to the porosity of the structure,

$$\phi \sim \frac{D^2 Y}{XYW} \quad \ldots (27)$$

where the dimensions X and Y are nearly equal, *cf.* Figures 2 and 3. From Equations (26, 27) and the Be definition[22] we deduce the form of the dimensionless mass flow rate,

$$M = \frac{\dot{m} Y}{\alpha \rho \phi^2 W^2} \quad \ldots (28)$$

From this follows the dimensionless definition of the pumping power,

$$\tilde{W} = \frac{\mathbf{P} Y^3}{\alpha^2 \mu \phi^2 W^2} \quad \ldots (29)$$

Figure 6 shows the relationship between M and $\tilde{R}_{max}$. The overall thermal resistance decreases monotonically as M increases. The slope of the tangent to the envelope of the resistance curves is negative, and is similar to the slope of the envelopes shown in Fig. 5.

Figure 7 shows the same information in terms of global thermal resistance *versus* pumping power. The recommended design (p)

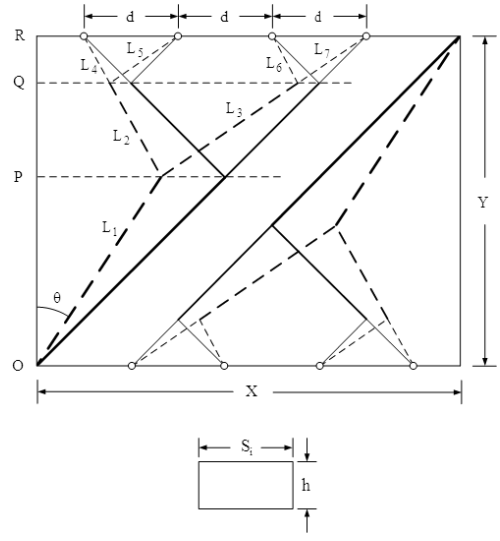


Figure 8 Line-to-line trees with non-parallel trunks, and the angle θ than can be optimised.

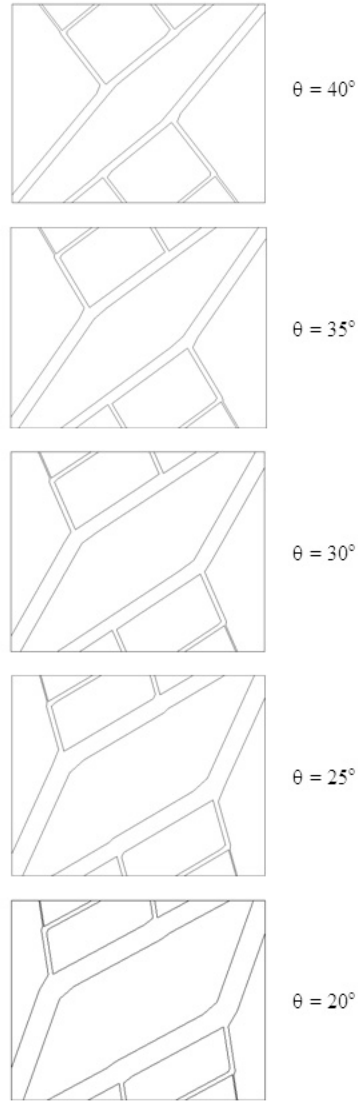


Figure 9. Five examples of line-to-line trees with non-parallel trunks with different angles θ and asymmetric bifurcations.

https://doi.org/10.1017/S0001924000003067 Published online by Cambridge University Press

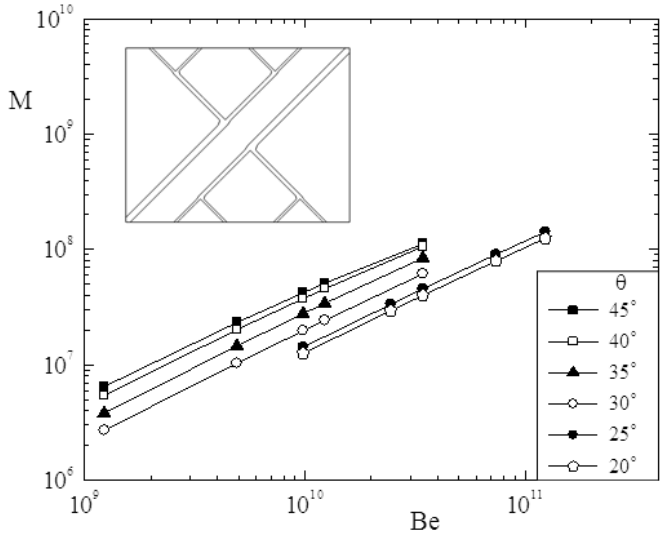


Figure 10 Dimensionless mass flow rates in six designs with two levels of bifurcation.

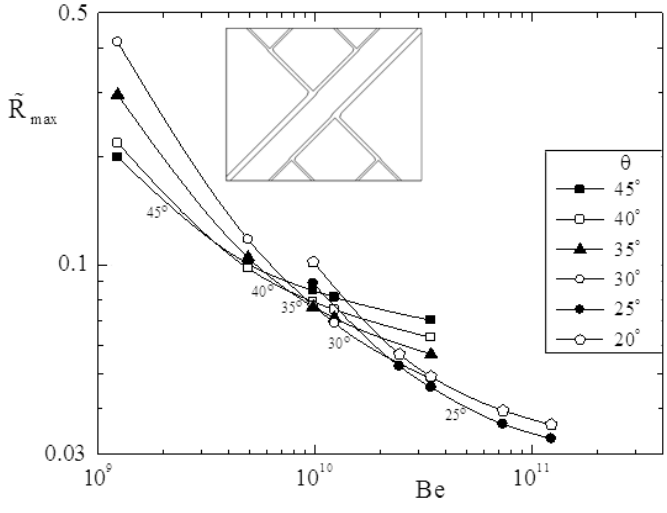


Figure 11. The effect of pressure drop number on the global thermal resistance of designs with two levels of bifurcation.

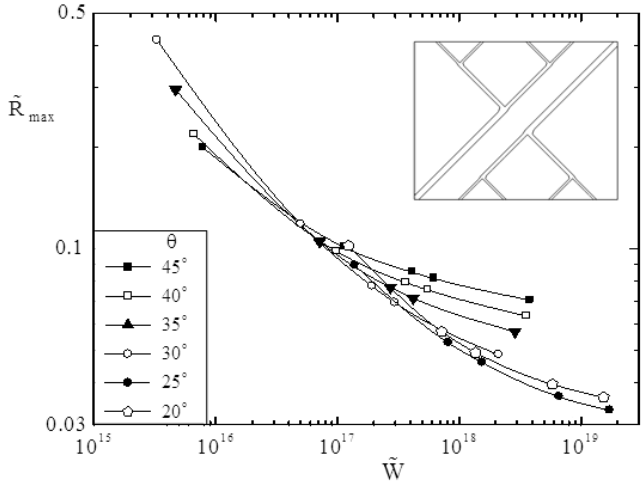


Figure 12. The effect of the pumping power on the global thermal resistance of designs with two levels of bifurcation.

depends on the application, that is on the specified available pumping power. The intersections of constant-p curves are essential, because they indicate the applications ($\tilde{W}$) for which there is a choice (or a transition) between two architectures, p and $p + 1$. Tree-shaped structures with more pairing levels become more attractive in the direction of increasing pumping power. For example, the $\tilde{R}_{max}(\tilde{W})$ curves with $p = 3$ and 4 intersect $\tilde{W} \cong 3{\cdot}8 \times 10^{19}$ indicating that when the available pumping power $\tilde{W}$ is less than $3{\cdot}8 \times 10^{19}$ the tree design with $p = 3$ is superior to the design with $p = 4$. When $\tilde{W}$ is less than $6{\cdot}3 \times 10^{17}$ the design with $p = 2$ is better than the design with $p = 3$, etc.

5.0 ASYMMETRIC LINE-TO-LINE TREES

The thermal performance of the tree designs is impeded by a peculiarity of the line to line trees: the large area A (Fig. 2) is not vascularised, and when Be is larger, this area serves as home for a larger hot spot (e.g., Fig. 4). A solution designed to correct this deficiency of the dendritic designs is presented in this section.

In Fig. 8 the design with tree with two pairing levels has one degree of freedom (θ) which allows it to depart from Fig. 2 and generate an asymmetric tree-tree architecture. The triangles (L_4, L_5, d) and (L_6, L_7, d) are the same, therefore $L_4 = L_6$ and $L_5 = L_7$. The smallest channel L_4 has a square cross-section, which has the smallest hydraulic diameter and channel width. In other words, S_4 and S_5 are smaller than S_6 and S_7 although L_4 and L_5 are the same as L_6 and L_7 respectively. Note also that S_2 is smaller than S_7. The reason the channel L_4 has the smallest hydraulic diameter is that the area between trees alternating with upside down trees increases (see Fig. 9) when θ decreases. So the arrangement of the channels with larger hydraulic diameters (L_1, L_3, L_7) relieves the concentration of heat on the area. Table 3 shows the geometrical features of Fig. 8, which were determined based on the generalisation of the Hess-Murray rule for bifurcations where the two daughter channels are not equal to each other [1,25]:

$$S_1 = S_2\left[1+\left(\frac{L_3}{L_2}\right)^2\right]^{2/3} \quad \ldots (30)$$

$$S_2 = h\left[1+\left(\frac{L_5}{L_4}\right)^2\right]^{2/3} \quad \ldots (31)$$

$$S_3 = S_2\left(\frac{L_3}{L_2}\right)^2 \quad \ldots (32)$$

$$S_4 = h \quad \ldots (33)$$

$$S_5 = h\left(\frac{L_5}{L_4}\right)^2 \quad \ldots (34)$$

$$S_6 = \frac{S_3}{\left[1+\left(\frac{L_7}{L_6}\right)^2\right]^{2/3}} \quad \ldots (35)$$

$$S_7 = S_6\left(\frac{L_7}{L_6}\right)^2 \quad \ldots (36)$$

We evaluated the thermo-fluid performance of asymmetric trees with two pairing levels, which have the same global features (X, Y, W, d, V_c, ϕ, $\tilde{k}$). Figure 10 shows the behavior of dimensionless flow conductance with respect to Be. The asymmetric tree configuration was varied by decreasing θ from 45° to 20° in steps of 5°. The flow

https://doi.org/10.1017/S0001924000003067 Published online by Cambridge University Press

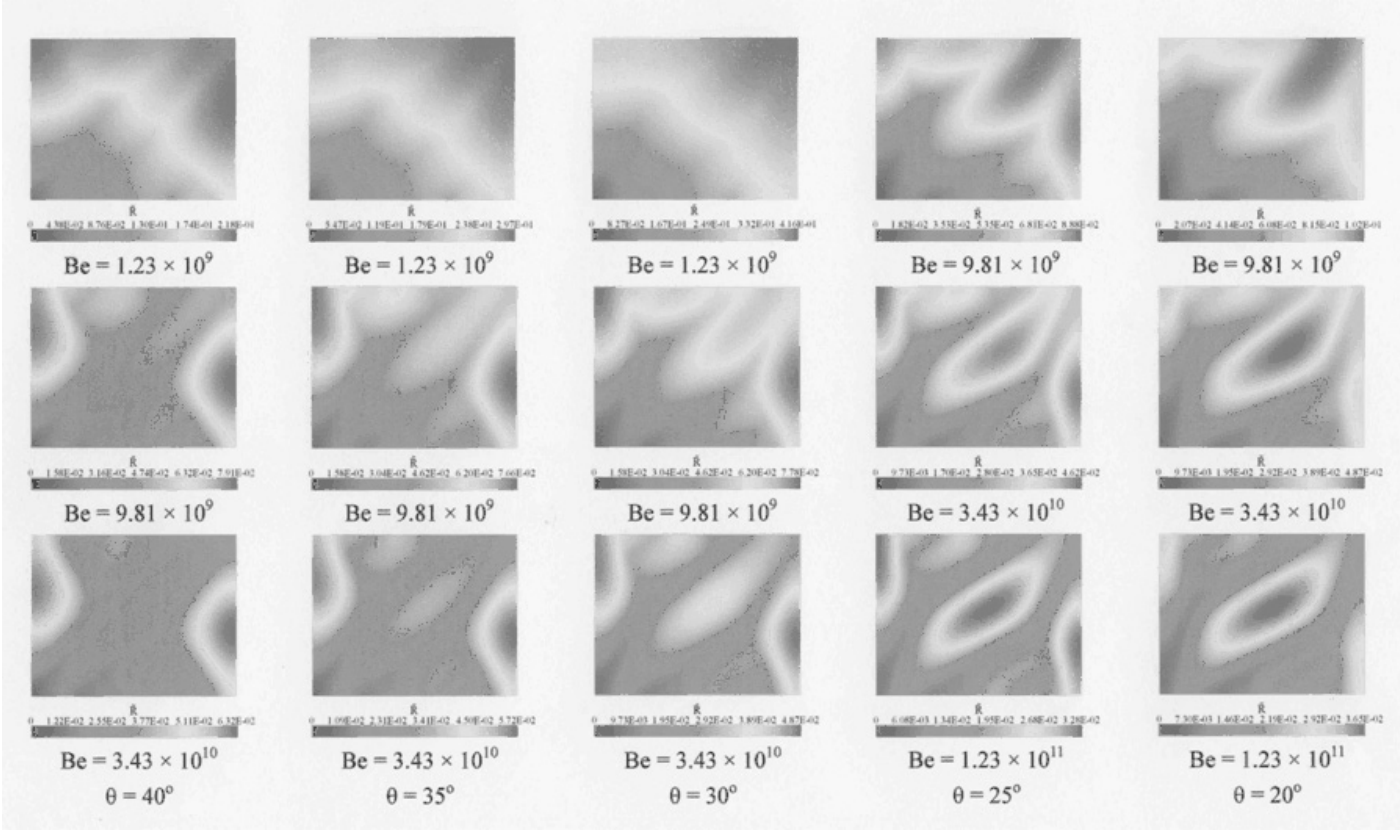


Figure 13. The distribution of temperature in the designs shown in Fig. 9.

conductance decreases when θ decreases because the ratio of channel width to height (S_i/h) increases, as shown in Table 3.

Figures 11 and 12 show the same data in terms of global thermal resistance *versus* *Be* and $\tilde{W}$. In Fig. 11 the thermal performance of trees improves as *Be* increases and as θ decreases. On the envelope of the curves for the trees, the best θ value decreases as *Be* increases. When $\tilde{R}_{max}$ is plotted against $\tilde{W}$, Fig. 12, the trend with respect to θ becomes less clear.

The effect of θ on the temperature distribution of tree structures is illustrated in Fig. 13. When θ decreases, the hot spots migrate from the largest interstitial area to the area between the two tree trunks.

6.0 COMPARISON WITH PARALLEL-PLATE CHANNELS

The thermo-fluid performance of line-to-line trees, which in Figs. 5-7 was documented for one class of vascularised materials ($\phi = 0{\cdot}02$, $\tilde{k} = 24$) can be extended over a wider domain by performing the heat and fluid flow simulations for other combinations of ϕ and $\tilde{k}$. More immediate at this stage is the question of whether any of the documented tree structures are more effective in the two-objective sense (low $\tilde{R}_{max}$ and low $\tilde{W}$, Fig. 7) than classical structures that employ arrays of parallel channels. In the limit where the parallel channels are sufficiently small and numerous, their thermo-fluid performance approaches that of a single thin sheet of fluid that flows through two parallel plates placed on the upper surface of the slab (Fig. 14). The parallel-plate channel architecture has the same global features (X, Y, W, V_c, ϕ, $\tilde{k}$) as the line-to-line tree.

The geometry of the parallel-plate sheet heated uniformly from above is cooled by a flow aligned with Y as shown in Fig. 14. The coolant is a stream of single phase $\dot{m}'$ (kg/s m) and initial temperature T_{min}. The flow regime is Poiseuille because the thickness of the parallel-plate sheet (δ) is sufficiently smaller than slab depth (W) in other words, $\phi << \delta/W$. The porosity and total pressure drop

Table 3
Geometrical features of the tree-tree architecture of Fig. 8, with reference to d = 0·5cm (ϕ = 0·02)

θ	*i*	S_i (mm)	L_i (mm)	*Area* (mm^2)	D_h (mm)
	1	0·86	13·1	0·18	0·33
	2	0·42	6·4	0·087	0·28
	3	0·65	7·9	0·13	0·31
40°	4	0·21	3·2	0·043	0·21
	5	0·32	3·9	0·066	0·25
	6	0·32	3·2	0·066	0·25
	7	0·49	3·9	0·10	0·29
	1	1·4	11·5	0·18	0·24
	2	0·43	5·5	0·055	0·20
	3	1.2	9·3	0·16	0·24
30°	4	0·13	2·7	0·017	0·13
	5	0·38	4·6	0·049	0·19
	6	0·38	2·7	0·049	0·19
	7	1·1	4·6	0·14	0·23
	1	1·7	11·0	0·18	0·20
	2	0·42	5·2	0·045	0·17
	3	1·5	9·9	0·16	0·20
25°	4	0·11	2·6	0·011	0·11
	5	0·39	4·9	0·041	0·17
	6	0·39	2·6	0·041	0·17
	7	1·4	4·9	0·15	0·20

https://doi.org/10.1017/S0001924000003067 Published online by Cambridge University Press

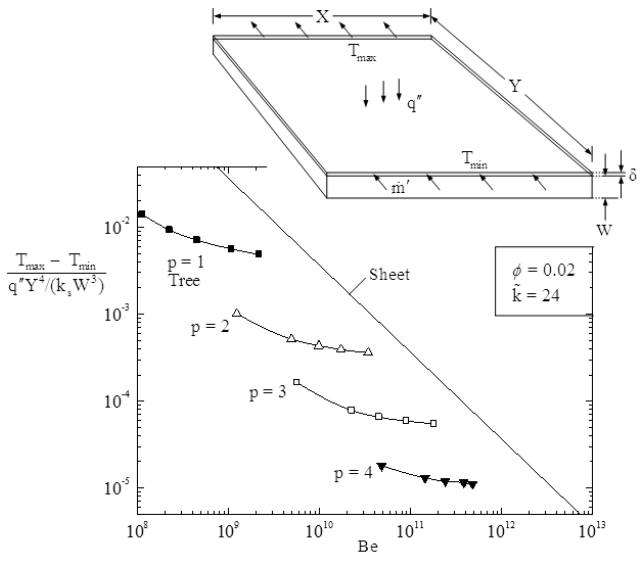


Figure 14. Comparison between the two-objective performance of tree-shaped designs (Fig. 5) and the corresponding performance of a design with cooling provided by a single sheet of fluid in Poiseuille flow.

between the inlet and the outlet of the channel are;

$$\phi = \frac{\delta}{W} \quad \ldots (37)$$

$$\frac{\Delta P}{\dot{m}'} = \frac{12\nu Y}{\phi^3 W^3} \quad \ldots (38)$$

When the channel is sufficiently thin with respect to W, the maximum temperature of coolant (T_{max}) is approximately the same as the wall material. The hot spot (T_{max}) occurs at the exit, and it is dictated by the first law written for the channel as a control volume

$$\dot{m}' c_p \left(T_{max} - T_{min}\right) = q'' Y \quad \ldots (39)$$

From Equations (22) and (23) follows the relationship between R_{max} and Be,

$$Be \cdot \tilde{R}_{max} \left(\frac{W}{Y}\right)^2 = 12 \frac{\tilde{k}}{\phi^3} \quad \ldots (40)$$

This relation appears as a straight line in Fig. 14, where on the ordinate we plotted the new group $R_{max}(W/Y)^2 = (T_{max} - T_{min})(k_s W^3)/(q'' Y^4)$. On this figure we added the results obtained for tree designs (Fig. 5), one curve for each number of pairing levels p. Because the desirable design domain is in the lower-left corner of the figure, it is clear that the tree designs outperform the sheet design throughout the Be range considered in this study. If Be is specified, then there is a best tree complexity (p) that delivers the smallest excess temperature at the hot spot, $T_{max} - T_{min}$. The recommended p value is finite (moderate), not maximal. For example, if $Be \sim 10^{10}$, then the recommended tree design has three levels of pairing, and the hot-spot excess temperature is ten times smaller than the level achievable with the fluid sheet design.

The comparison presented in this section is only for orientation. The sheet flow configuration was used because its performance can be evaluated analytically. Important to keep in mind is that the sheet flow configuration overestimates both the thermal and flow friction performance of actual designs. The actual R_{max} value will be higher than in Equation (40) because of the additional thermal resistance between T_{max} (in the solid, which receive the heat flux) and the temperature of the sheet fluid. The actual Be value will be higher than in Equation (40) because the cross-sections of parallel channels have lateral walls that pose friction, unlike the cross-section of the single sheet flow.

7.0 CONCLUSIONS

The numerical simulations and generation of flow configurations reported in this paper documented the thermo-fluid characteristics of line-to-line tree vasculatures of the type proposed in Fig. 2. We reported this for fluid flow and conjugate heat transfer in three dimensions, while accounting for pressure losses at the junctions.

Important is the trend revealed by all the results, which point toward greater performance in the direction where the vascular designs are endowed with more freedom to morph. We showed that the large areas with high temperatures are suppressed when the trunks of adjacent trees are allowed to become non-parallel, and when the bifurcations become asymmetric. More freedom to morph is also available toward higher numbers of bifurcations, where more length scales and angles can be varied and optimised.

This route of design discovery deserves to be pursued further so that the merits of tree-shaped vascular designs can be fully explored and put into practice.

One of the reviewers of the original manuscript made two observations that help explain better the context in which the constructal design with vascular structures is new and useful. We discuss these two observations here:

(*i*) The reviewer said that the advantages of dendritic flow structures were known in biology [26] and geophysics[27] a few years before the constructal law[2,7]. For example, the comparison between radial channels and tree-shaped channels as two models of river basins argues in favour of the tree-shaped design[27]. The difference between this slightly older work and the constructal law[2,7] is the difference between empiricism and pure theory. It is a big difference. The earlier work[26,27] is modeling, which begins with observing nature, making a simple model (a facsimile) of the observed, and then analysing the model by pursuing an ad-hoc objective such as the minimisation of flow resistance. The ad-hoc is not a universal principle.

With the constructal law, nature is not observed, copied or modelled. The first step is the mental viewing − the principle of how things should be − from which the flow configuration (evolution, construction, direction, no end) is deduced. This is made very clear in the second constructal-law paper[7], where it is also shown that the single channel (i.e. the radial design, not the dendritic) is the easier flowing configuration when the flow domain is sufficiently small. Furthermore, the constructal law holds across the board, from geophysical to biological flow designs, not in *ad-hoc* fashion. There are many optimality statements (different, and often contradictory) that have been invoked to account *ad-hoc* for features of design in nature, and all their results have been predicted based on the constructal law[6].

(*ii*) The reviewer also said that there are alternative methodologies that address the advantages of dendritic topologies such as 'fractal theory' and 'topology optimisation'[28-30]. First, the constructal law is not a methodology, and not a method of optimisation. It is a law of generation of configuration, and it has been translated into predictions by employing many different methodologies (analytical, trial and error, numerical, genetic algorithms, experimental, etc.). Second, topology optimisation refers to the numerical optimisation of configuration by invoking *ad-hoc* an optimality objective. This is not an alternative to the constructal law, unless the *ad-hoc* objective is more general than the constructal law (it is not[6]).

(*iii*) Third, there is no such thing as 'fractal theory'. Fractal geometry is a descriptive method, not a theory. The fractal geometrist sees a natural tree, selects one algorithm out of an infinity of algorithms, repeats it a few times and makes a tree-like drawing. Just like a painter who picks the right paint and brush. This is description, not prediction. And this is not even a

https://doi.org/10.1017/S0001924000003067 Published online by Cambridge University Press

fractal drawing, because the algorithm was repeated only a few times (so that the drawing could be made, and seen). The drawing would be 'fractal' only if the algorithm were to be repeated ad infinitum. The fact that natural tree architectures have finite and modest numbers of branching levels is a fact of 'design in nature' that is predictable from the constructal law[27]. More branching levels in larger systems, and fewer in smaller systems, all the way to no branchings at all in sufficiently small systems, cf. (*i*) above.

ACKNOWLEDGMENT

This research was supported by the Air Force Office of Scientific Research based on a grant for 'Constructal Technology for Thermal Management of Aircraft'. We thank Dr Victor Giurgiutiu (AFOSR) and Dr David Moorhouse (Air Force Research Laboratory) for the advice and guidance that he gives us in this research direction. Jaedal Lee's work at Duke University was sponsored by the Korea Research Foundation Grant funded by the Korean Government (MOEHRD) (KRF-2006-612- D00011). Jaedal Lee acknowledges with gratitude the continued advice received from Prof Moohawn Kim of Pohang University of Science and Technology (POSTECH), Pohang, South Korea.

REFERENCES

1. BEJAN, A. and LORENTE, S. *Design with Constructal Theory*, 2008, Wiley, Hoboken, USA.
2. BEJAN, A. *Advanced Engineering Thermodynamics*, 1997, 2nd ed, Wiley, New York, USA.
3. BEJAN, A. *Shape and Structure, from Engineering to Nature*, Cambridge University Press, 2000, Cambridge, UK.
4. BEJAN, A. and LORENTE, S. Constructal theory of generation of configuration in nature and engineering, *J Appl Phys*, 2006, **100**, 041301.
5. HEITOR REIS, A. Constructal theory: from engineering to physics, and how flow systems develop shape and structure, *Appl Mechanics Reviews*, 2006, **59**, pp 269-282.
6. BEJAN, A. and MARDEN, J.H. The constructal unification of biological and geophysical design, *Physics of Life Reviews*, 2008, doi:10.1016/j.plrev.2008.12.002.
7. BEJAN, A. Constructal-theory network of conducting paths for cooling a heat generating volume, *Int J Heat Mass Transfer*, 1997, **40**, pp 799-816.
8. CHEN, Y and CHENG, P. Heat transfer and pressure drop in fractal tree-like microchannel nets, *Int J Heat Mass Transfer*, 2002, **45**, pp 2643-2648.
9. CHEN, Y and CHENG, P. An experimental investigation on the thermal efficiency of fractal tree-like microchannel nets, *Int Comm Heat Mass Transfer*, 2005, **32**, pp 931-938.
10. PENCE, D.V. Reduced pumping power and wall temperature in microchannel heat sinks with fractal-like branching channel networks, *Microscale Thermophys Eng*, 2002, **6**, pp 316-330.
11. ALHARBI, A.Y., PENCE, D.V. and CULLION, R.N. Fluid flow through microscale fractal-like branching channel networks, *J Fluids Eng,* 2003, **125**, pp 1051-1057.
12. SENN, S.M. and POULIKAKOS, D. Laminar mixing, heat transfer and pressure drop in tree-like microchannel nets and their application for thermal management in polymer electrolyte fuel cells, *J Power Sources*, 2004, **130**, pp 178-191.
13. SENN, S.M. and POULIKAKOS, D. Tree network channels as fluid distributors constructing double-staircase polymer electrolyte fuel cells, *J Appl Phys,* 2004, **96**, pp 842-852.
14. WANG K.-M., LORENTE, S. and BEJAN, A. Vascularized networks with two optimized channel sizes, *J Phys D: Appl Phys*, 2006, **39**, pp 3086-3096.
15. KIM, S.W., LORENTE, S. and BEJAN, A. Vascularized materials: tree-shaped flow architectures matched canopy to canopy, *J Appl Phys,* 2006, **100**, 063525.
16. LORENTE, S. and BEJAN, A. Heterogeneous porous media as multiscale structures for maximum flow access, *J Appl Phys*, 2006, **100**, 114909.
17. LORENTE, S., WECHSATOL, W. and BEJAN, A. Tree-shaped flow structures designed by minimizing path lengths, *Int J Heat Mass Transfer*, 2002, **45**, pp 3299-3312.
18. LORENTE, S. and BEJAN, A. Svelteness, freedom to morph, and constructal multi-scale flow structures, *Int J Thermal Sci*, 2005, **44**, pp 1123-1130.
19. MURRAY, C.D. The physiological principle of minimal work in the vascular system, and the cost of blood-volume, *Proc Acad Natl Sci,* 1926, **12**, pp 207-214.
20. WEIBEL, E.R. *Symmorphosis: On Form and Function in Shaping Life*, Harvard University Press, 2000, Harvard, MA, USA, pp 16-17.
21. ZHANG, H., LORENTE, S. and BEJAN, A. Vascularization with trees that alternate with upside-down trees, *J Appl Phys*, 2007, **101**, 094904.
22. BHATTACHARJEE, S. and GROSSHANDLER, W.L. The formation of a wall jet near a high temperature wall under microgravity environment, ASME HTD, 1988, **96**, pp 711-716.
23. PETRESCU, S. Comments on the optimal spacing of parallel plates cooled by forced convection, *Int J Heat Mass Transfer*, 1994, **37**, pp 1283-1283.
24. STARCCM+ (Version 1.04) basics, CD-adapco Company.
25. BEJAN, A. *Advanced Engineering Thermodynamics*, 3rd ed, Wiley, Hoboken, NJ, USA, 2006, problem 13.20, p 840.
26. LABARBERA, M. Principles of design of fluid transport systems in zoology, *Science*, 1990, **249**, pp 992-1000.
27. RODRIGUEZ-ITURBE, I. and RINALDO, A. *Fractal River Basins*, Cambridge University Press, Cambridge, UK, 2007.
28. BENDSOE, M.P. and SIGMUND, O. *Topology Optimization: Theory, Methods and Applications*, Springer, Berlin, Germany, 2003.
29. GERSBORG-HANSEN, A. BENDSOE, M.P. and SIGMUND, O. Topology optimization of heat conduction problems using the finite volume method, *Structural Multidisciplinary Optimization*, 2006, **31**, pp 251-259.
30. BRUNS, T.E. Topology optimization of convection-dominated, steady-state heat transfer problems, *Int J Heat Mass Transfer*, 2007, **50**, pp 2859-2873.

https://doi.org/10.1017/S0001924000003067 Published online by Cambridge University Press